Chapter 8

Robust Adaptive Fuzzy Control for a Class of Switching Power Converters

Cheng-Lun Chen

Additional information is available at the end of the chapter

http://dx.doi.org/10.5772/67895

Abstract

This chapter provides the reader with a control-centric modeling and analysis approach along with a nonlinear control design for a class of switching power converters. A comprehensive model combining the respective state variable models of the interval subsystems is established. Comparison with PSpice simulation justifies the credibility of the model. Based on this model, internal/BIBO stability can be studied for each interval subsystem. Moreover, controllability and observability can also be analyzed to help determine subsequent control configuration. The established model is further investigated for advanced control design, i.e., robust adaptive fuzzy control.

Keywords: adaptive fuzzy control, dc-dc power converter, modeling, switching power converter

1. Introduction

Switching power converters are increasingly taking over conventional linear power converters due to their being compact, lightweight, high efficiency, and larger input voltage range. With the rapid advancement and popularity of personal computers, mobile communication devices, and automotive electronics, the need for stability and efficiency of converters is rising. Among the switching power converters, the phase-shifted pulse-width modulated (PSPWM) full-bridge soft switched power converter [1, 2] and corresponding alteration [3–8] have become a widely used circuit topology due to various beneficial characteristics, e.g., reduction of switching losses and stresses, and elimination of primary snubbers. The circuit is capable of high switching frequency operation with improved power density and conversion efficiency.

Feedback control has been incorporated into switching power converters to not only stabilize, but also improve the performance robustness of the output voltage. In spite of its advantageous features, feedback control for soft switched PSPWM full-bridge converters is still confined to simple linear time-invariant design, e.g., proportional-integral (PI) or lead-lag compensators based on a linearized model [9–12]. As pointed out by [13, 14], due to the increased number of topological stages and the PWM duty cycle being affected by input voltage, output voltage, and load current, the dynamics of a PSPWM full-bridge converter is much more sophisticated than that of a simple buck converter. A trade-off needs to be made regarding whether a simple model (e.g., linearized model) or a complex one (e.g., switched model) is to be established for the purpose of control design.

For model-based control design, a mathematical model of appropriate sophistication and capture of desired dynamics is normally the initial step. Such models can usually be obtained by simplifying a complex model, i.e., model reduction, or linearizing a nonlinear around specified operation point. For design of linear controllers, transfer function is a matured modeling tool. For more advanced control design, state variable model is usually a prerequisite. Various modeling approaches for switching power converters of complex topology have been proposed in the literature [15–20]. Most of them have been successful in terms of modeling the "local" behavior (i.e., small signal model) or analysis of the fundamental characteristics. However, few of the results can carry over to the next stage of control design. To be specific, a variety of crucial information for control design cannot be retrieved from those "not control centric" modeling approaches. That essential information includes stability, controllability, and observability of the open-loop system.

This chapter will provide the reader with a control-centric modeling and analysis approach along with robust adaptive fuzzy control design for switching power converters of complex topology and resort to PSPWM full-bridge power converters as a design example. The outline of the chapter is as follows:

Sections 2 and 3 demonstrate how to establish a control-centric mathematical model for a PSPWM full-bridge soft switched power converter system. The set of differential equations and the corresponding state variable model are established for each operation interval. The subsystem models for all intervals are integrated to form a comprehensive model. Numerical simulation of the model is performed and compared to that of the corresponding PSpice model to verify its validity. Section 4 will perform stability analysis for the system. Specifically, stability analysis is performed for each interval subsystem (of the established model) to determine whether the subsystem is internally/BIBO stable. Section 5 will conduct controllability/observability analysis for the system. Controllability and observability of the subsystems are analyzed to determine which signals/variables can actually be manipulated by control effort and which can be estimated using output feedback control structure. The established comprehensive model is further exploited for advanced control design. For example, by getting rid of uncontrollable and unobservable variables and dynamics, an LPV gain-scheduling control design may be conducted as in Ref. [21]. Model reduction and robust adaptive fuzzy control design are presented in Sections 6 and 7. Conclusion and future work are given in Section 8.

http://dx.doi.org/10.5772/67895

2. Control-centric mathematical model

In this section, operation of a PSPWM full-bridge dc-dc power converter will be briefly described. Note that there are eight operation intervals. Due to switching, operation of adjacent intervals is discontinuous. This implies that the parameters and initial conditions change when the converter switches. It will be demonstrated how a comprehensive control-oriented state variable model for each operation interval can be established for subsequent analysis and numerical simulation. The circuit diagram of the converter is shown in **Figure 1**. **Figure 2** is the waveform timing for various signals in the converter, where $i_{L_{lK}}$ is the primary current, v_{ab} is the voltage between a and b, i_L is the secondary current, v_s is the secondary voltage, Q_A,Q_B,Q_C, and Q_D are the four switches, ΔD is the duty cycle loss, and ZVS delay is the dead time.

2.1. Positive half cycle: trailing-leg (passive-to-active) transition $(t_0 \sim t_1)$

During this operation interval, only Q_D is conducting. **Figure 3** shows the equivalent circuit of state 1. Initial conditions are $v_{C_A}(t_0) = v_i$, $v_{C_B}(t_0) = 0$, $v_{C_C}(t_0) = v_i$, and $v_{C_D}(t_0) = 0$. During this interval, C_A is discharging and C_B is charging until v_{C_A} equals zero. Q_A is turned on at zero voltage. Utilizing Kirchhoff's voltage law (KVL) and Kirchhoff's current law (KCL), we arrive at the following set of differential equations:

$$\frac{dv_{C_A}(t)}{dt} = \frac{i_{L_{lk}}}{C_A + C_B}, \frac{dv_{C_B}(t)}{dt} = -\frac{i_{L_{lk}}}{C_A + C_B}, \frac{dv_{C_C}(t)}{dt} = 0, \frac{dv_{C_D}(t)}{dt} = 0 \tag{1}$$

$$-\frac{di_{L_{lk}}}{dt} = \frac{di_L}{dt} = \frac{-1}{n^2 L_{lk} + L} v_C + \frac{n}{n^2 L_{lk} + L} v_{C_A} + \frac{-n}{n^2 L_{lk} + L} v_i, \quad \frac{dv_C(t)}{dt} = \frac{1}{C} i_L - \frac{1}{RC} v_C \tag{2}$$

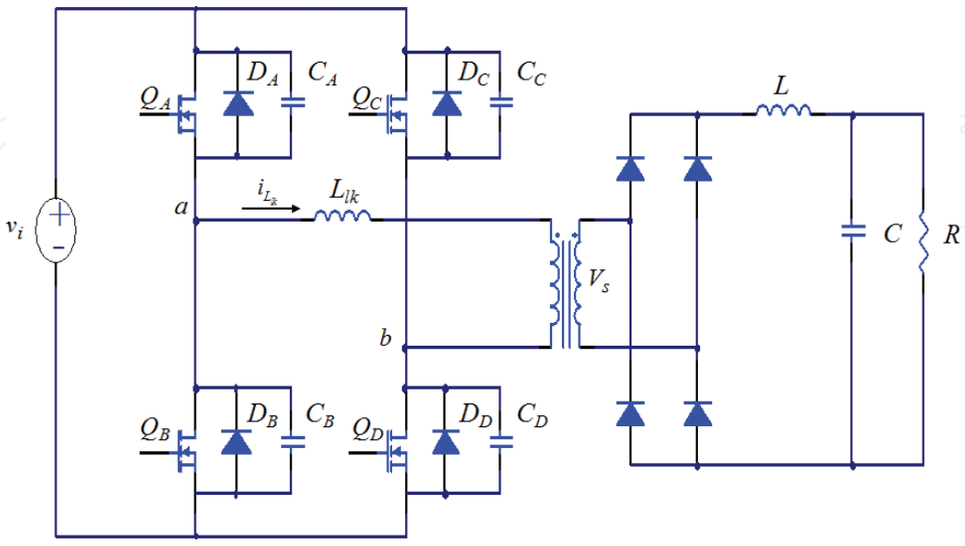

Figure 1. Circuit topology of a PSPWM full-bridge converter.

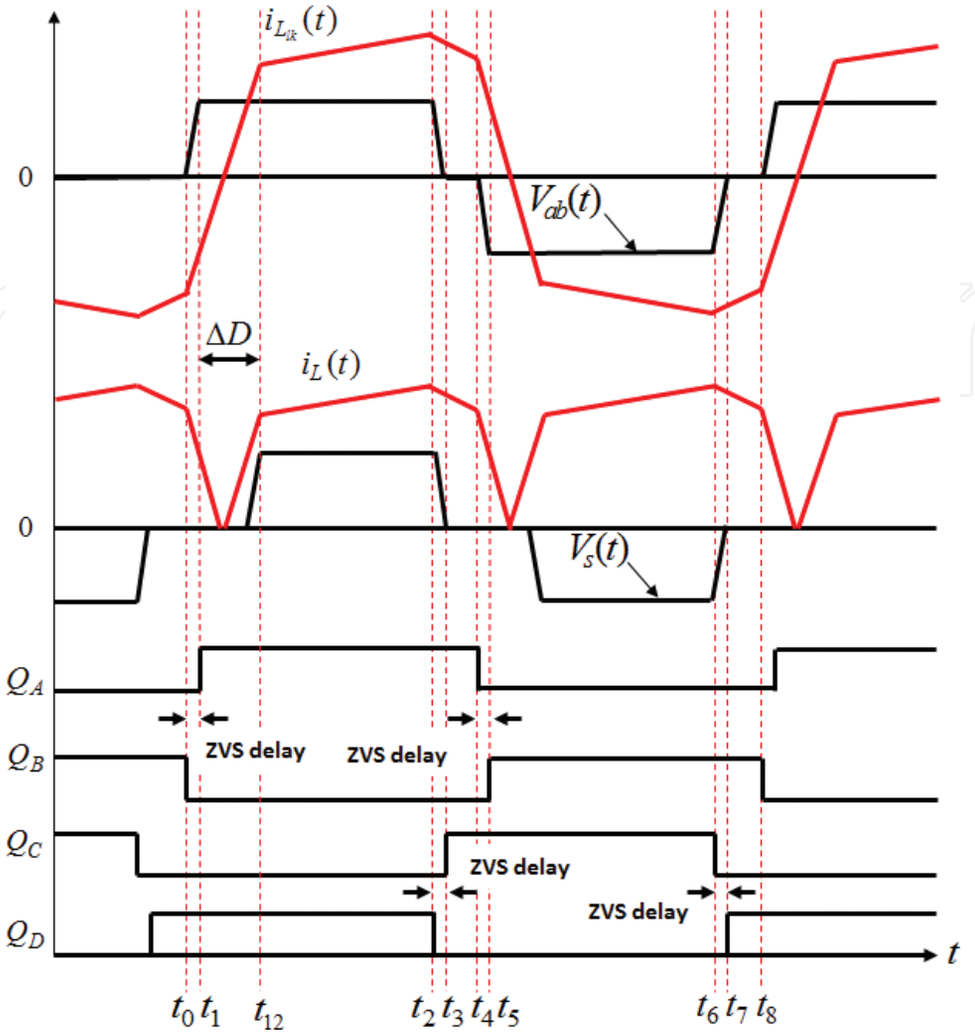

Figure 2. Waveform timing for a PSPWM full-bridge converter.

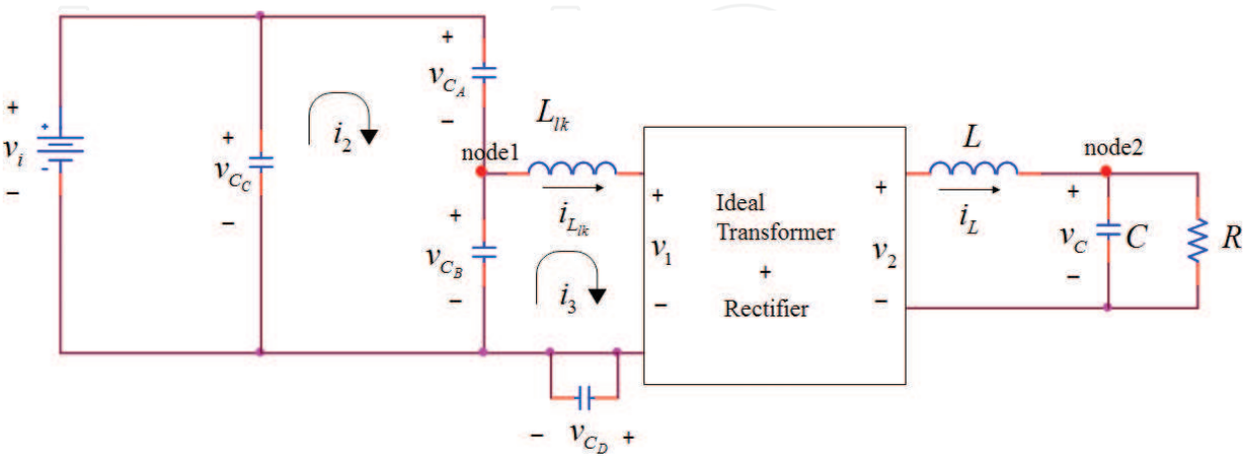

Figure 3. The equivalent circuit of operation interval 1 (t_0~t_1).

Define $\vec{x}(t) = [\, i_{L_{lK}}(t) \quad i_L(t) \quad v_C(t) \quad v_{C_A}(t) \quad v_{C_B}(t) \quad v_{C_C}(t) \quad v_{C_D}(t) \,]^T$, where $i_{L_{lK}}$ is leakage inductance current, i_L is inductance current, v_C is output voltage, v_{C_A} is the voltage across C_A, v_{C_B} is the voltage across C_B, v_{C_C} is the voltage across C_C, and v_{C_D} is the voltage across C_D. Therefore, a state variable model can be obtained as follows:

$$\dot{\vec{x}}(t) = \begin{bmatrix} 0 & 0 & \frac{n}{n^2L_{lk}+L} & \frac{-n^2}{n^2L_{lk}+L} & 0 & 0 & 0 \\ 0 & 0 & \frac{-1}{n^2L_{lk}+L} & \frac{n}{n^2L_{lk}+L} & 0 & 0 & 0 \\ 0 & \frac{1}{C} & -\frac{1}{RC} & 0 & 0 & 0 & 0 \\ \frac{1}{C_A+C_B} & 0 & 0 & 0 & 0 & 0 & 0 \\ -\frac{1}{C_A+C_B} & 0 & 0 & 0 & 0 & 0 & 0 \\ 0 & 0 & 0 & 0 & 0 & 0 & 0 \\ 0 & 0 & 0 & 0 & 0 & 0 & 0 \end{bmatrix} \vec{x}(t) + \begin{bmatrix} \frac{n^2}{n^2L_{lk}+L} \\ \frac{-n}{n^2L_{lk}+L} \\ 0 \\ 0 \\ 0 \\ 0 \\ 0 \end{bmatrix} v_i(t) \tag{3}$$

where v_i is input voltage, $N_2/N_1 = n$ is the transformer turns ratio, L is inductance, C is capacitance, and R is resistance.

2.2. Positive half cycle: active region $(t_1 \sim t_2)$

During this operation interval, Q_A and Q_D are conducting. Initially, due to leakage inductance, the secondary side will experience a short period of "no energy" passing through, called duty cycle loss. **Figure 4** shows the equivalent circuit for this period. Initial conditions are $v_{C_A}(t_1) = 0$, $v_{C_B}(t_1) = v_i$, $v_{C_C}(t_1) = v_i$, and $v_{C_D}(t_1) = 0$. Similarly, we may derive a set of differential equations and the corresponding state variable model for this short period is

$$\dot{\vec{x}}(t) = \begin{bmatrix} 0 & 0 & 0 & 0 & 0 & 0 & 0 \\ 0 & 0 & -\frac{1}{L} & 0 & 0 & 0 & 0 \\ 0 & \frac{1}{C} & -\frac{1}{RC} & 0 & 0 & 0 & 0 \\ 0 & 0 & 0 & 0 & 0 & 0 & 0 \\ 0 & 0 & 0 & 0 & 0 & 0 & 0 \\ 0 & 0 & 0 & 0 & 0 & 0 & 0 \\ 0 & 0 & 0 & 0 & 0 & 0 & 0 \end{bmatrix} \vec{x}(t) + \begin{bmatrix} \frac{1}{L_{lk}} \\ 0 \\ 0 \\ 0 \\ 0 \\ 0 \\ 0 \end{bmatrix} v_i(t) \tag{4}$$

After the short period of duty cycle loss, energy passes through the transformer again. **Figure 5** shows the equivalent circuit. Initial conditions are $v_{C_A}(t_{12}) = 0$, $v_{C_B}(t_{12}) = v_i$, $v_{C_C}(t_{12}) = v_i$, and $v_{C_D}(t_{12}) = 0$. We may derive a set of differential equations and the corresponding set of differential equations and state variable model are

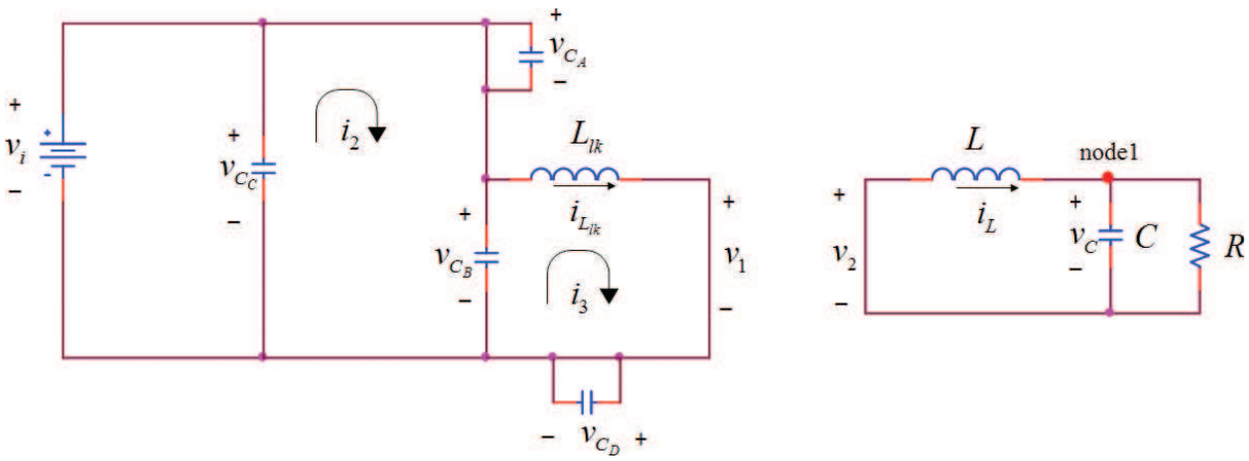

Figure 4. The equivalent circuit of the period of duty cycle loss (t_1~t_2).

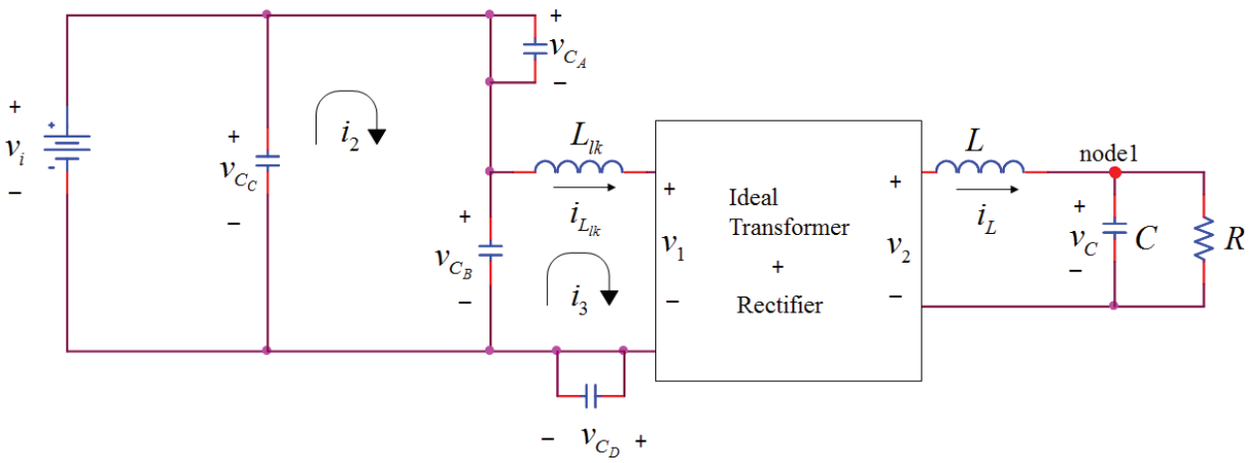

Figure 5. The equivalent circuit of operation interval 2 (t_1~t_2).

$$\dot{\vec{x}}(t) = \begin{bmatrix} 0 & 0 & -\frac{n}{n^2L_{lk}+L} & 0 & 0 & 0 & 0 \\ 0 & 0 & -\frac{1}{n^2L_{lk}+L} & 0 & 0 & 0 & 0 \\ 0 & \frac{1}{C} & -\frac{1}{RC} & 0 & 0 & 0 & 0 \\ 0 & 0 & 0 & 0 & 0 & 0 & 0 \\ 0 & 0 & 0 & 0 & 0 & 0 & 0 \\ 0 & 0 & 0 & 0 & 0 & 0 & 0 \\ 0 & 0 & 0 & 0 & 0 & 0 & 0 \end{bmatrix} \vec{x}(t) + \begin{bmatrix} \frac{n^2}{n^2L_{lk}+L} \\ \frac{n}{n^2L_{lk}+L} \\ 0 \\ 0 \\ 0 \\ 0 \\ 0 \end{bmatrix} v_i(t) \tag{5}$$

The duration of duty cycle loss may be derived based on falling range of i_L is equal to rising range of i_L, i.e.,

$$\frac{t_{passive}}{n^2L_{lk}+L}v_C+\frac{\Delta D}{L}v_C=\left(\frac{-1}{n^2L_{lk}+L}v_C+\frac{n}{n^2L_{lk}+L}v_i\right)\times(t_{active}-\Delta D)\phi=\frac{t_{passive}}{t_{passive}+t_{active}}\times 180^\circ \quad (6)$$

where ΔD is duty cycle loss time, $t_{passive}$ is the time of passive region, t_{active} is the time of active region, and ϕ is the difference of phase between Q_A and Q_C.

2.3. Positive half cycle: leading-leg (active-to-passive) transition $(t_2 \sim t_3)$

During this operation interval, only Q_A is conducting. Initial conditions are $v_{C_A}(t_2)=0$, $v_{C_B}(t_2)=v_i$, $v_{C_C}(t_2)=v_i$, and $v_{C_D}(t_2)=0$. In this interval, C_C is discharging and C_D is charging until v_{C_C} equals zero. Q_C is turned on at zero voltage. Applying KVL/KCL in a similar way, we obtain

$$\dot{\vec{x}}(t)=\begin{bmatrix} 0 & 0 & -\frac{n}{n^2L_{lk}+L} & 0 & 0 & 0 & -\frac{n^2}{n^2L_{lk}+L} \\ 0 & 0 & -\frac{1}{n^2L_{lk}+L} & 0 & 0 & 0 & -\frac{n}{n^2L_{lk}+L} \\ 0 & \frac{1}{C} & -\frac{1}{RC} & 0 & 0 & 0 & 0 \\ 0 & 0 & 0 & 0 & 0 & 0 & 0 \\ 0 & 0 & 0 & 0 & 0 & 0 & 0 \\ -\frac{1}{C_C+C_D} & 0 & 0 & 0 & 0 & 0 & 0 \\ \frac{1}{C_C+C_D} & 0 & 0 & 0 & 0 & 0 & 0 \end{bmatrix}\vec{x}(t)+\begin{bmatrix} \frac{n^2}{n^2L_{lk}+L} \\ \frac{n}{n^2L_{lk}+L} \\ 0 \\ 0 \\ 0 \\ 0 \\ 0 \end{bmatrix}v_i(t) \quad (7)$$

2.4. Positive half cycle: Passive region $(t_3 \sim t_4)$

During this interval, Q_A and Q_C are conducting. Initial conditions are $v_{C_A}(t_3)=0$, $v_{C_B}(t_3)=v_i$, $v_{C_C}(t_3)=0$, and $v_{C_D}(t_3)=v_i$. Applying KVL/KCL in a similar way, we obtain

$$\dot{\vec{x}}(t)=\begin{bmatrix} 0 & 0 & -\frac{n}{n^2L_{lk}+L} & 0 & 0 & 0 & 0 \\ 0 & 0 & -\frac{1}{n^2L_{lk}+L} & 0 & 0 & 0 & 0 \\ 0 & \frac{1}{C} & -\frac{1}{RC} & 0 & 0 & 0 & 0 \\ 0 & 0 & 0 & 0 & 0 & 0 & 0 \\ 0 & 0 & 0 & 0 & 0 & 0 & 0 \\ 0 & 0 & 0 & 0 & 0 & 0 & 0 \\ 0 & 0 & 0 & 0 & 0 & 0 & 0 \end{bmatrix}\vec{x}(t) \quad (8)$$

2.5. Negative half cycle

The subsequent four operation intervals basically "mirror" those in positive cycle. Therefore, the derivations are omitted for brevity.

3. Solution and numerical simulation

Numerical simulation based on a typical PSPWM full-bridge power converter circuit (with parameters: transformer turns ratio n = 0.5, $V_i = 160$ volt, $V_o = 50$ volt, R = 6 Ω, C = 940 μF, L = 300 μH, $L_{lk} = 20\mu H$, $C_A = C_B = C_C = C_D = 5nF$, $f_s = 50$ kHz) in our laboratory is performed. A "realistic" model of the circuit is built using PSpice, and the developed mathematical model is realized using MATLAB/Simulink. Comparison of the simulation results validates the correctness and effectiveness of the established model.

4. Stability analysis

4.1. Zero-state response

A SISO system (A, B, C) with proper rational transfer function $G(s) = C(sI - A)^{-1}B$ is BIBO stable if and only if every pole of $G(s)$ has a negative real part or, equivalently, lies inside the left-half s-plane. For both positive and negative half cycles, we can obtain the following transfer function for each operation interval:

- Trailing-leg (passive-to-active) transition:

$$G_1 = \frac{-nR(C_A + C_B)s}{RC(C_A + C_B)(n^2L_{lk} + L)s^3 + (C_A + C_B)(n^2L_{lk} + L)s^2 + (R(C_A + C_B) + n^2RC)s + n^2} \quad (9)$$
$$pole = p11, p12, p13 \text{ (in complicated form)}$$

- Active region (duty cycle loss): $G_{2loss} = 0$
- Active region:

$$G_2 = \frac{nR}{RC(n^2L_{lk} + L)s^2 + (n^2L_{lk} + L)s + R}$$
$$pole = \frac{-(n^2L_{lk} + L) \pm \sqrt{(n^2L_{lk} + L)^2 - 4R^2C(n^2L_{lk} + L)}}{2RC(n^2L_{lk} + L)} \quad (10)$$

- Leading-leg (active-to-passive) transition:

$$G_3 = \frac{nR(C_C + C_D)s}{RC(C_C + C_D)(n^2L_{lk} + L)s^3 + (C_C + C_D)(n^2L_{lk} + L)s^2 + (R(C_C + C_D) + n^2RC)s + n^2} \quad (11)$$
$$pole = p31, p32, p33 \text{(in complicated form)}$$

- Passive region: no input:

Due to "mirroring" operation, corresponding intervals in positive and negative half cycles will have the same transfer function. The pole location for the operation interval of trailing-leg and

http://dx.doi.org/10.5772/67895

leading-leg transition depends further on the values of the circuit elements. The poles for the operation interval of active region have negative real parts due to

$$(n^2L_{lk}+L) > \sqrt{(n^2L_{lk}+L)^2 - 4R^2C(n^2L_{lk}+L)} \tag{12}$$

Hence, the system is BIBO stable within this interval. Note that there is pole/zero cancelation for all intervals, which implies that each interval subsystem is either uncontrollable or unobservable.

4.2. Zero-input response

The equation $\dot{x} = Ax$ is marginally stable if and only if all eigenvalues of A have zero or negative real parts and those with zero real parts are simple root of the minimal polynomial of A. The equation $\dot{x} = Ax$ is asymptotically stable if and only if all eigenvalues of A have negative real parts. For both positive and negative half cycles, we can obtain the following set of eigenvalues for each operation interval:

- Trailing-leg (passive-to-active) transitions:

$$A_1 = \begin{bmatrix} 0 & 0 & \frac{n}{n^2L_{lk}+L} & \frac{-n^2}{n^2L_{lk}+L} & 0 & 0 & 0 \\ 0 & 0 & \frac{-1}{n^2L_{lk}+L} & \frac{n}{n^2L_{lk}+L} & 0 & 0 & 0 \\ 0 & \frac{1}{C} & \frac{-1}{RC} & 0 & 0 & 0 & 0 \\ \frac{1}{C_A+C_B} & 0 & 0 & 0 & 0 & 0 & 0 \\ \frac{-1}{C_A+C_B} & 0 & 0 & 0 & 0 & 0 & 0 \\ 0 & 0 & 0 & 0 & 0 & 0 & 0 \\ 0 & 0 & 0 & 0 & 0 & 0 & 0 \end{bmatrix}, \lambda = 0, 0, 0, 0, \lambda 11, \lambda 12, \lambda 13 \tag{13}$$

- Active region (duty cycle loss):

$$\lambda = 0, 0, 0, 0, 0, \frac{-1 \pm \sqrt{(L-4R^2C)/L}}{2RC} \tag{14}$$

- Active region:

$$\lambda = 0, 0, 0, 0, 0, \frac{-(n^2L_{lk}+L) \pm \sqrt{(n^2L_{lk}+L)^2 - 4R^2C(n^2L_{lk}+L)}}{2RC(n^2L_{lk}+L)} \tag{15}$$

- Leading-leg (active-to-passive) transitions:

$$\lambda = 0, 0, 0, 0, \lambda 31, \lambda 32, \lambda 33(\text{in complicated form}) \tag{16}$$

- Passive region:

$$\lambda = 0, 0, 0, 0, 0, \frac{-(n^2 L_{lk} + L) \pm \sqrt{(n^2 L_{lk} + L)^2 - 4R^2 C(n^2 L_{lk} + L)}}{2RC(n^2 L_{lk} + L)} \tag{17}$$

Since all intervals have zero eigenvalue, we need to determine whether zero is a simple root of the minimal polynomial of A. The minimal polynomial (in x) for each operation interval (positive or negative half cycle) is summarized as follows:

- Trailing-leg (passive-to-active) transitions:

$$x^4 + \frac{1}{RC}x^3 + \frac{n^2 C + C_A + C_B}{C(C_A + C_B)(n^2 L_{lk} + L)}x^2 + \frac{n^2}{RC(C_A + C_B)(n^2 L_{lk} + L)}x \tag{18}$$

- Active region (duty cycle loss):

$$x^3 + \frac{1}{RC}x^2 + \frac{1}{LC}x \tag{19}$$

- Active region:

$$x^3 + \frac{1}{RC}x^2 + \frac{1}{C(n^2 L_{lk} + L)}x \tag{20}$$

- Leading-leg (active-to-passive) transitions:

$$x^4 + \frac{1}{RC}x^3 + \frac{n^2 C + C_C + C_D}{C(C_C + C_D)(n^2 L_{lk} + L)}x^2 + \frac{n^2}{RC(C_C + C_D)(n^2 L_{lk} + L)}x \tag{21}$$

- Passive region:

$$x^3 + \frac{1}{RC}x^2 + \frac{1}{C(n^2 L_{lk} + L)}x \tag{22}$$

Although all operation intervals have different state matrix (A), corresponding intervals in positive and negative half cycles actually possess the same set of eigenvalues. The eigenvalues for the operation interval of trailing-leg and leading-leg transition depend further on the values of the circuit elements. Both intervals of active (including duty cycle loss) and passive region are marginally stable due to

$$n^2L_{lk}+L>\sqrt{(n^2L_{lk}+L)^2-4R^2C(n^2L_{lk}+L)},\quad 1>\sqrt{\frac{L-4R^2C}{L}} \tag{23}$$

and zero is the simple root of the minimal polynomial.

5. Controllability/observability analysis

The stability analysis indicates that all interval subsystems have uncontrollable or unobservable modes. We may decompose the state variable model of each subsystem into controllable and uncontrollable parts, and follow by decomposing each part into observable and unobservable parts to obtain

$$\begin{bmatrix}\dot{\bar{x}}_{co}\\ \dot{\bar{x}}_{c\bar{o}}\\ \dot{\bar{x}}_{\bar{c}o}\\ \dot{\bar{x}}_{\bar{c}\bar{o}}\end{bmatrix}=\left[\begin{array}{c|ccc}\bar{A}_{co} & 0 & \bar{A}_{13} & 0\\ \hline \bar{A}_{21} & \bar{A}_{c\bar{o}} & \bar{A}_{23} & \bar{A}_{24}\\ 0 & 0 & \bar{A}_{\bar{c}o} & 0\\ 0 & 0 & \bar{A}_{43} & \bar{A}_{\bar{c}\bar{o}}\end{array}\right]\begin{bmatrix}\bar{x}_{co}\\ \bar{x}_{c\bar{o}}\\ \bar{x}_{\bar{c}o}\\ \bar{x}_{\bar{c}\bar{o}}\end{bmatrix}+\begin{bmatrix}\bar{B}_{co}\\ \bar{B}_{c\bar{o}}\\ 0\\ 0\end{bmatrix}u,\ y=\left[\begin{array}{c|ccc}\bar{C}_{co} & 0 & \bar{C}_{\bar{c}o} & 0\end{array}\right]\begin{bmatrix}\bar{x}_{co}\\ \bar{x}_{c\bar{o}}\\ \bar{x}_{\bar{c}o}\\ \bar{x}_{\bar{c}\bar{o}}\end{bmatrix} \tag{24}$$

The observability matrices of the controllable part for each operation interval (positive or negative half cycle) are summarized as follows:

- Trailing-leg (passive-to-active) transition:

$$O_{c1}=\begin{bmatrix}0 & \dfrac{-n}{C(n^2L_{lk}+L)} & \dfrac{n}{RC^2(n^2L_{lk}+L)}\\ \dfrac{-n}{C(n^2L_{lk}+L)} & \dfrac{n}{RC^2(n^2L_{lk}+L)} & \dfrac{n(n^2C+C_A+C_B)}{C^2(C_A+C_B)(n^2L_{lk}+L)^2}-\dfrac{n}{R^2C^3(n^2L_{lk}+L)}\\ \dfrac{n}{RC^2(n^2L_{lk}+L)} & oc1.1 & oc1.2\end{bmatrix} \tag{25}$$

- Active region (duty cycle loss):

$$O_{c2loss}=[0] \tag{26}$$

- Active region:

$$O_{c2}=\begin{bmatrix}0 & \dfrac{n}{C(n^2L_{lk}+L)}\\ \dfrac{n}{C(n^2L_{lk}+L)} & \dfrac{-n}{RC^2(n^2L_{lk}+L)}\end{bmatrix} \tag{27}$$

- Leading-leg (active-to-passive) transitions:

$$O_{c3} = \begin{bmatrix} 0 & \frac{n}{C(n^2L_{lk}+L)} & \frac{-n}{RC^2(n^2L_{lk}+L)} \\ \frac{n}{C(n^2L_{lk}+L)} & \frac{-n}{RC^2(n^2L_{lk}+L)} & \frac{n}{R^2C^3(n^2L_{lk}+L)} - \frac{n(n^2C+C_C+C_D)}{C^2(C_C+C_D)(n^2L_{lk}+L)^2} \\ \frac{-n}{RC^2(n^2L_{lk}+L)} & oc3.1 & oc3.2 \end{bmatrix} \quad (28)$$

Table 1 summarizes the rank of the observability matrix. The state variables of both controllable and observable are listed in **Table 2**. Since equivalent transformation does not affect the eigenvalues, Eq. (24) has the same set of eigenvalues as in stability analysis. For the operation intervals of trailing/leading leg and active region, uncontrollable or unobservable states (v_{C_A},v_{C_B},v_{C_C}, and v_{C_D}) are marginally stable corresponding to zero eigenvalue. Therefore, those states will stay constant within those intervals, which matches what is observed in numerical simulation. For the intervals of duty cycle loss and passive region, uncontrollable (i_L, v_C) states are asymptotically stable, which also matches what is observed during simulation.

	Interval	**Rank**
Positive half cycle	Trailing-leg (passive-to-active) transitions	3
	Active region (duty cycle loss)	0
	Active region	2
	Leading-leg (active-to-passive) transitions	3
Negative half cycle	Trailing-leg (passive-to-active) transitions	3
	Active region (duty cycle loss)	0
	Active region	2
	Leading-leg (active-to-passive) transitions	3

Table 1. Rank of the observability matrix for the controllable part.

	Interval	**Controllable and observable**
Positive half cycle	Trailing-leg (passive-to-active) transitions	i_L, v_C, v_{C_B}
	Active region	i_L, v_C
	Leading-leg (active-to-passive) transitions	i_L, v_C, v_{C_D}
Negative half cycle	Trailing-leg (passive-to-active) transitions	i_L, v_C, v_{C_B}
	Active region	i_L, v_C
	Leading-leg (active-to-passive) transitions	i_L, v_C, v_{C_D}

Table 2. State variables of both controllable and observable.

http://dx.doi.org/10.5772/67895

6. Model reduction

The goal is to obtain a low dimensional model that encompasses the imperative response characteristics of the comprehensive model. The reduced model is then utilized for subsequent control design. For control of the "steady-state" response, we neglect the transition intervals and take only the active region and passive region into consideration. Define d is duty cycle (ON) of the converter and $d' = 1 - d$ (OFF). Assuming that $L_{lk} \ll L$, we may derive the following differential inclusion model

$$\begin{bmatrix} \frac{di_L(t)}{dt} \\ \frac{dv_o(t)}{dt} \end{bmatrix} = \begin{bmatrix} 0 & -\frac{1}{L} \\ \frac{1}{C} & -\frac{1}{RC} \end{bmatrix} \begin{bmatrix} i_L(t) \\ v_o(t) \end{bmatrix} + \begin{bmatrix} \frac{nd}{L} \\ 0 \end{bmatrix} v_i(t) \tag{29}$$

Let $x_1 = i_L, x_2 = v_o, u = d, y = v_o$

$$\begin{bmatrix} \dot{x}_1 \\ \dot{x}_2 \end{bmatrix} = \begin{bmatrix} 0 & \frac{-1}{L} \\ \frac{1}{C} & \frac{-1}{RC} \end{bmatrix} \begin{bmatrix} x_1 \\ x_2 \end{bmatrix} + \begin{bmatrix} \frac{nv_i}{L} \\ 0 \end{bmatrix} u, \ddot{y} = \frac{-1}{RC^2} x_1 + \left(\frac{1}{R^2C^2} - \frac{1}{LC} \right) x_2 + \frac{nv_i}{LC} u \tag{30}$$

7. Indirect adaptive fuzzy control for uncertain switching power converters subject to external disturbances

In the following, we propose a robust adaptive fuzzy tracking controller for the PSPWM full-bridge soft switched power converter. Although the controller is designed based on the reduced model, its effectiveness and performance are subsequently verified with the comprehensive model.

Indirect adaptive fuzzy control with sliding model

Based on the input-output linearization concept, Eq. (30) can be represented by

$$y^{(2)} = f(\boldsymbol{x}) + g(\boldsymbol{x})u, f(\boldsymbol{x}) = \frac{-1}{RC^2} x_1 + \left(\frac{1}{R^2C^2} - \frac{1}{LC} \right) x_2, \ g(\boldsymbol{x}) = \frac{nv_i}{LC} \tag{31}$$

The control objective is to force y to follow a given bounded reference signal y_m, under the constraint that all signals involved must be bounded. Let $e = y_m - y$, $\boldsymbol{e} = (e, \dot{e})^T$ and $\boldsymbol{k} = (k_2, k_1)^T$ be such that all roots of the polynomial $s^2 + k_1 s + k_2$ are in the open left half-plane. If the functions f and g are known, then the control law

$$u = \frac{1}{g(\boldsymbol{x})} [-f(\boldsymbol{x}) + y_m{}^{(2)} + \boldsymbol{k}^T \boldsymbol{e}] \tag{32}$$

applied to Eq. (31) results in

$$e^{(2)} + k_1\dot{e} + k_2 e = 0 \tag{33}$$

which implies that $\lim_{t\to\infty} e(t) = 0$ a main objective of control.

However, f and g are unknown. We replace f and g in Eq. (32) by the fuzzy logic systems $\hat{f}(\boldsymbol{x}|\boldsymbol{\theta}_f)$ and $\hat{g}(\boldsymbol{x}|\boldsymbol{\theta}_g)$. The resulting control law

$$u_c = \frac{1}{\hat{g}(\boldsymbol{x}|\boldsymbol{\theta}_g)}\left[-\hat{f}(\boldsymbol{x}|\boldsymbol{\theta}_f) + {y_m}^{(2)} + \boldsymbol{k}^T\boldsymbol{e}\right] \tag{34}$$

is the so-called certainty equivalent controller. We use

$$u = u_c + u_s \tag{35}$$

where the additional control term u_s is called a supervisory control for stability. Substituting Eq. (35) into Eq. (31), we obtain the error equation

$$\dot{\boldsymbol{e}} = \Lambda_c\boldsymbol{e} + \boldsymbol{b}_c\left[\hat{f}(\boldsymbol{x}|\boldsymbol{\theta}_f) - f(\boldsymbol{x}) + \left(\hat{g}(\boldsymbol{x}|\boldsymbol{\theta}_g) - g(\boldsymbol{x})\right)u_c - g(\boldsymbol{x})u_s\right] \tag{36}$$

where

$$\Lambda_c = \begin{bmatrix} 0 & 1 \\ -k_2 & -k_1 \end{bmatrix}, \qquad b_c = \begin{bmatrix} 0 \\ 1 \end{bmatrix} \tag{37}$$

Since Λ_c is a stable matrix ($|sI - \Lambda_c| = s^n + k_1 s^{(n-1)} + \cdots + k_n$ which is stable), we know that there exists a unique positive definite symmetric $n\times n$ matrix P which satisfies the Lyapunov equation:

$${\Lambda_c}^T P + P\Lambda_c = -Q \tag{38}$$

where Q is an arbitrary 2×2 positive definite matrix. Let $V_e = \frac{1}{2}\boldsymbol{e}^T P\boldsymbol{e}$, in order for $x_i = y_m^{(i-1)} - e^{(i-1)}$ to be bounded, we require that V_e must be bounded, which means we require that $\dot{V}_e \le 0$ when V_e is greater than a large constant $\overline{V}$. Using Eq. (35) and Eq. (38), we have

$$\begin{aligned} \dot{V}_e &= -\frac{1}{2}\boldsymbol{e}^T Q\boldsymbol{e} + \boldsymbol{e}^T P\boldsymbol{b}_c[(\hat{f}(\boldsymbol{x}|\boldsymbol{\theta}_f) - f(\boldsymbol{x})) + (\hat{g}(\boldsymbol{x}|\boldsymbol{\theta}_g) - g(\boldsymbol{x}))u_c - g(\boldsymbol{x})u_s] \\ &\le -\frac{1}{2}\boldsymbol{e}^T Q\boldsymbol{e} + |\boldsymbol{e}^T P\boldsymbol{b}_c|[|(\hat{f}(\boldsymbol{x}|\boldsymbol{\theta}_f)| + |f(\boldsymbol{x})| + |\hat{g}(\boldsymbol{x}|\boldsymbol{\theta}_g)u_c| + |g(\boldsymbol{x})u_c|] - \boldsymbol{e}^T P\boldsymbol{b}_c g(\boldsymbol{x})u_s \end{aligned} \tag{39}$$

In order to design the u_s such that the right-hand side of Eq. (39) is not positive, we need to know the bounds of f and g. That is, we have to make the following assumption.

http://dx.doi.org/10.5772/67895

Assumption: We can determine functions $f^U(\boldsymbol{x})$, $g^U(\boldsymbol{x})$ and $g_L(\boldsymbol{x})$such that $|f(\boldsymbol{x})| \le f^U(\boldsymbol{x})$ and $g_L(\boldsymbol{x}) \le g(\boldsymbol{x}) \le g^U(\boldsymbol{x})$ for $\boldsymbol{x} \in R^2$, where $f^U(\boldsymbol{x}) < \infty$, $g^U(\boldsymbol{x}) < \infty$, and $g_L(\boldsymbol{x}) > 0$ for $\boldsymbol{x} \in R^2$.

Based on $f^U(\underline{\boldsymbol{x}})$, $g^U(\underline{\boldsymbol{x}})$ and $g_L(\underline{\boldsymbol{x}})$, and by observing Eq. (39), we choose the supervisory control u_s as

$$u_s = \begin{cases} \operatorname{sgn}(\boldsymbol{e}^T P \boldsymbol{b}_c) \dfrac{1}{g_L(\boldsymbol{x})} [|\hat{f}(\boldsymbol{x}|\boldsymbol{\theta}_f)| + |f^U(\boldsymbol{x})| + |\hat{g}(\boldsymbol{x}|\boldsymbol{\theta}_g) u_c| + |g^U(\boldsymbol{x}) u_c|], & V_e \ge \overline{V} \\ 0, & V_e \le \overline{V} \end{cases} \tag{40}$$

Substituting Eq. (40) into Eq. (39) and considering the case $V_e > \overline{V}$, we have

$$\begin{aligned} \dot{V}_e &\le -\frac{1}{2} \boldsymbol{e}^T Q \boldsymbol{e} + |\boldsymbol{e}^T P \boldsymbol{b}_c| [|\hat{f}| + |f| + |\hat{g} u_c| + |g u_c| - \frac{g}{g_L} (|\hat{f}| + f^U + |\hat{g} u_c| + |g^U u_c|)] \\ &\le -\frac{1}{2} \boldsymbol{e}^T Q \boldsymbol{e} < 0 \end{aligned} \tag{41}$$

In summary, using the control Eq. (35), we can guarantee that $V_e \le \overline{V} < \infty$. Since P is positive definite, the boundedness of V_e implies the boundedness of $\boldsymbol{e}$, which in turn implies the boundedness of $\boldsymbol{x}$.

We employ the following fuzzy logic system:

$$\hat{f}(\boldsymbol{x}|\boldsymbol{\theta}_f) = \sum_{l=1}^{M} \theta_l \xi_l(\boldsymbol{x}) \ = \boldsymbol{\theta}^T \boldsymbol{\xi}(\boldsymbol{x}) \tag{42}$$

where $\boldsymbol{\theta} = (\theta_1, \ldots, \theta_M)^T$, $\xi(\boldsymbol{x}) = (\xi_1(\boldsymbol{x}), \ldots, \xi_M(\boldsymbol{x}))^T$, $\xi_l(\boldsymbol{x})$ is the fuzzy basis function defined by

$$\xi_l(\boldsymbol{x}) = \prod_{i=1}^{2} \mu_{F_i^l}(x_i) \Big/ \sum_{l=1}^{M} \prod_{i=1}^{2} \mu_{F_i^l}(x_i) \tag{43}$$

θ_l are adjustable parameters, and $\mu_{F_i^l}$ are given membership functions.

We present the detailed design steps of the adaptive fuzzy controller.

- Step 1 Define p_i fuzzy sets $A_i^{l_i} (l_i = 1, 2, \ldots, p_i)$ for variable $x_i (i = 1, 2)$
- Step 2 There are $\prod_{i=1}^{2} p_i$ rules to construct fuzzy systems $\hat{f}(\boldsymbol{x}|\boldsymbol{\theta}_f)$:

$$\textit{if } x_1 \textit{ is } A_1^{l_1} \textit{ and } x_2 \textit{ is } A_2^{l_2}, \quad \textit{then } \hat{f} \textit{ is } E^{l_1 \ldots l_2}$$

There are $\prod_{i=1}^{2} q_i$ rules to construct fuzzy systems $\hat{g}(\boldsymbol{x}|\boldsymbol{\theta}_g)$:

$$\textit{if } x_1 \textit{ is } B_1^{l_1} \textit{ and } x_2 \textit{ is } B_2^{l_2}, \quad \textit{then } \hat{g} \textit{ is } H^{l_1 \ldots l_2}$$

Using product-inference rule, singleton fuzzifier, and center average defuzzifier, we obtain

$$\hat{f}(\boldsymbol{x}|\boldsymbol{\theta}_f) = \boldsymbol{\theta}_f^T \boldsymbol{\xi}_f(\boldsymbol{x}), \hat{g}(\boldsymbol{x}|\boldsymbol{\theta}_g) \ = \boldsymbol{\theta}_g^T \boldsymbol{\xi}_g(\boldsymbol{x}) \tag{44}$$

where

$$\xi_f^l(\boldsymbol{x}) = \frac{\prod_{i=1}^2 \mu_{A_i^l}(x_i)}{\sum_{l=1}^{p_1 \times p_2} \prod_{i=1}^2 \mu_{A_i^l}(x_i)}, \xi_g^l(\boldsymbol{x}) = \frac{\prod_{i=1}^2 \mu_{B_i^l}(x_i)}{\sum_{l=1}^{p_1 \times p_2} \prod_{i=1}^2 \mu_{B_i^l}(x_i)} \tag{45}$$

Our next task is to develop an adaptive law to adjust the parameters in the fuzzy logic systems for the purpose of forcing the tracking error to converge to zero.

Define

$$\begin{aligned} \boldsymbol{\theta}_f^* &= \arg\min_{\theta_f}[sup_{\boldsymbol{x} \in R^2}|\hat{f}(\boldsymbol{x}|\boldsymbol{\theta}_f) - f(\boldsymbol{x})|] \\ \boldsymbol{\theta}_g^* &= \arg\min_{\theta_g}[sup_{\boldsymbol{x} \in R^2}|\hat{g}(\boldsymbol{x}|\boldsymbol{\theta}_g) - g(\boldsymbol{x})|] \end{aligned} \tag{46}$$

Define the minimum approximation error

$$\omega = (\hat{f}(\boldsymbol{x}|\boldsymbol{\theta}_f^*) - f(\boldsymbol{x})) + (\hat{g}(\boldsymbol{x}|\boldsymbol{\theta}_g^*) - g(\boldsymbol{x}))u_c \tag{47}$$

Then the error equation can be rewritten as

$$\dot{\boldsymbol{e}} = \Lambda_c \boldsymbol{e} + \boldsymbol{b}_c[(\hat{f}(\boldsymbol{x}|\boldsymbol{\theta}_f)) - \hat{f}(\boldsymbol{x}|\boldsymbol{\theta}_f^*)) + (\hat{g}(\boldsymbol{x}|\boldsymbol{\theta}_g) - \hat{g}(\boldsymbol{x}|\boldsymbol{\theta}_g^*))u_c + \omega] \tag{48}$$

Substituting Eq. (43) into Eq. (47), we have

$$\dot{\boldsymbol{e}} = \Lambda_c \boldsymbol{e} + \boldsymbol{b}_c \omega + \boldsymbol{b}_c[(\boldsymbol{\theta}_f - \boldsymbol{\theta}_f^*)^T \boldsymbol{\xi}_f(\boldsymbol{x}) + (\boldsymbol{\theta}_g - \boldsymbol{\theta}_g^*)^T \boldsymbol{\xi}_g(\boldsymbol{x})u_c] \tag{49}$$

Consider the Lyapunov function candidate

$$V = \frac{1}{2}\boldsymbol{e}^T P \boldsymbol{e} + \frac{1}{2\gamma_1}(\boldsymbol{\theta}_f - \boldsymbol{\theta}_f^*)^T(\boldsymbol{\theta}_f - \boldsymbol{\theta}_f^*) + \frac{1}{2\gamma_2}(\boldsymbol{\theta}_g - \boldsymbol{\theta}_g^*)^T(\boldsymbol{\theta}_g - \boldsymbol{\theta}_g^*) \tag{50}$$

where γ_1 and $\gamma_2$are positive constants. The time derivative of Valong the trajectory of Eq. (48) is

$$\begin{aligned} \dot{V} = -\frac{1}{2}\boldsymbol{e}^T Q \boldsymbol{e} + \boldsymbol{e}^T P \boldsymbol{b}_c \omega + \frac{1}{\gamma_1}(\boldsymbol{\theta}_f - \boldsymbol{\theta}_f^*)^T[\dot{\boldsymbol{\theta}}_f + \gamma_1 \boldsymbol{e}^T P \boldsymbol{b}_c \boldsymbol{\xi}_f(x)] \\ + \frac{1}{\gamma_2}(\boldsymbol{\theta}_g - \boldsymbol{\theta}_g^*)^T[\dot{\boldsymbol{\theta}}_g + \gamma_2 e^T P b_c \boldsymbol{\xi}_g(\boldsymbol{x})u_c] \end{aligned} \tag{51}$$

If we choose the adaptive law

$$\dot{\boldsymbol{\theta}}_f = -\gamma_1 \boldsymbol{e}^T P \boldsymbol{b}_c \xi_f(\boldsymbol{x}), \dot{\boldsymbol{\theta}}_g = -\gamma_2 \boldsymbol{e}^T P \boldsymbol{b}_c \xi_g(\boldsymbol{x})u_c \tag{52}$$

then from Eq. (50) we have

$$\dot{V} = -\frac{1}{2}\boldsymbol{e}^T Q \boldsymbol{e} + e^T P \boldsymbol{b}_c \omega \tag{53}$$

This is the best we can hope to get because the term $\boldsymbol{e}^T P\boldsymbol{b}_c\omega$ is of the order of the minimum approximation error. If $\omega = 0$, that is, the searching spaces for $\hat{f}$ and $\hat{g}$ are so big that f and g are included in them, then we have $\dot{V} \le 0$. Eq. (51) cannot guarantee $\boldsymbol{\theta}_f$ and $\boldsymbol{\theta}_g$ are bounded, so we use projection algorithm. If the parameter vectors $\boldsymbol{\theta}_f$ and $\boldsymbol{\theta}_g$ are within the constraint sets or on the boundaries of the constraint sets but moving toward the inside of the constraint sets, then use the simple adaptive law Eq. (51). Otherwise, if the parameter vectors are on the boundaries of the constraint sets but moving toward the outside of the constraint sets, then use the projection algorithm to modify the adaptive law Eq. (51). such that the parameter vectors will remain inside the constraint sets.

$$\Omega_f = \left\{ \boldsymbol{\theta}_f \in R^{\prod_{i=1}^{2} p_i} \mid \|\boldsymbol{\theta}_f\| \le M_f \right\} \tag{54}$$

$$\Omega_g = \left\{ \boldsymbol{\theta}_g \in R^{\prod_{i=1}^{2} q_i} \mid 0 < \varepsilon \le \|\boldsymbol{\theta}_g\| \le M_g \right\} \tag{55}$$

where Ω_f and Ω_g are constraint sets for $\boldsymbol{\theta}_f$ and $\boldsymbol{\theta}_g$, M_f, M_g, ε are constants

$$\dot{\boldsymbol{\theta}}_f = \begin{cases} -\gamma_1 \boldsymbol{e}^T P\boldsymbol{b}_c \xi_f(x) & \text{if } (\|\boldsymbol{\theta}_f\| < M_f) \text{ or } (\|\boldsymbol{\theta}_f\| = M_f \text{ and } \boldsymbol{e}^T P\boldsymbol{b}_c \xi_f(\boldsymbol{x}) \ge 0) \\ P\{-\gamma_1 \boldsymbol{e}^T P\boldsymbol{b}_c \xi_f(x)\} & \text{if } (\|\boldsymbol{\theta}_f\| = M_f \text{ and } \boldsymbol{e}^T P\boldsymbol{b}_{cc} \xi_f(\boldsymbol{x}) < 0) \end{cases} \tag{56}$$

where the projection operator $P\{*\}$ is defined as

$$P\{-\gamma_1 \boldsymbol{e}^T P\boldsymbol{b}_c \xi_f(\boldsymbol{x})\} = -\gamma_1 \boldsymbol{e}^T P\boldsymbol{b}_c \xi_f(\boldsymbol{x}) + \gamma_1 \boldsymbol{e}^T P\boldsymbol{b}_c \frac{\boldsymbol{\theta}_f \boldsymbol{\theta}_f^T \xi_f(\boldsymbol{x})}{\|\boldsymbol{\theta}_f\|^2} \tag{57}$$

Whenever an element $\boldsymbol{\theta}_{gi}$ of $\boldsymbol{\theta}_g = \varepsilon$, use

$$\dot{\theta}_{gi} = \begin{cases} -\gamma_2 \boldsymbol{e}^T P\boldsymbol{b}_c \xi_{gi}(\boldsymbol{x}) u_c & \text{if } \boldsymbol{e}^T P\boldsymbol{b}_c \xi_{gi}(\boldsymbol{x}) u_c < 0 \\ 0 & \text{if } \boldsymbol{e}^T P\boldsymbol{b}_c \xi_{gi}(\boldsymbol{x}) u_c \ge 0 \end{cases} \tag{58}$$

where $\xi_{gi}(\boldsymbol{x})$ is the ith component of $\xi_g(\boldsymbol{x})$.

Otherwise, use

$$\dot{\boldsymbol{\theta}}_g = \begin{cases} -\boldsymbol{\gamma}_2 \boldsymbol{e}^T P\boldsymbol{b}_c \xi_g(\boldsymbol{x}) u_c & \text{if } (\|\boldsymbol{\theta}_g\| < M_g) \text{ or } (\|\boldsymbol{\theta}_g\| = M_g \text{ and } \boldsymbol{e}^T P\boldsymbol{b}_c \xi_g(\boldsymbol{x}) u_c \ge 0) \\ P\{-\gamma_2 \boldsymbol{e}^T P\boldsymbol{b}_c \xi_g(\boldsymbol{x})\} & \text{if } (\|\boldsymbol{\theta}_g\| = M_g \text{ and } \boldsymbol{e}^T P\boldsymbol{b}_c \xi_g(\boldsymbol{x}) u_c < 0) \end{cases} \tag{59}$$

where the projection operator $P\{*\}$ is defined as

$$P\{-\gamma_2 \boldsymbol{e}^T P\boldsymbol{b}_c \xi_g(\boldsymbol{x}) u_c\} = -\gamma_2 \boldsymbol{e}^T P\boldsymbol{b}_c \xi_g(\boldsymbol{x}) u_c + \gamma_2 \boldsymbol{e}^T P\boldsymbol{b}_c \frac{\boldsymbol{\theta}_g \boldsymbol{\theta}_g^T \boldsymbol{\xi}_g(\boldsymbol{x}) u_c}{\|\boldsymbol{\theta}_g\|^2} \tag{60}$$

Theorem:

1. $\|\boldsymbol{\theta}_f(t)\| \le M_f, \|\boldsymbol{\theta}_g(t)\| \le M_g$, all elements of $\boldsymbol{\theta}_g \ge \varepsilon$,

$$\|\boldsymbol{x}(t)\| \le \|\boldsymbol{y_m}\| + \left(\frac{2\overline{V}}{\lambda_{P\min}}\right)^{\frac{1}{2}} \tag{61}$$

$$|u(t)| \le \frac{1}{\varepsilon}\left(M_f + |y_m^2| + \|\boldsymbol{k}\|\left(\frac{2\overline{V}}{\lambda_{P\min}}\right)^{\frac{1}{2}}\right) + \frac{1}{g_L(\boldsymbol{x})}$$
$$\left[M_f + |f^U(\boldsymbol{x})| + \frac{1}{\varepsilon}(M_g + g^U)\left(M_f + |y_m^2| + \|\boldsymbol{k}\|\left(\frac{2\overline{V}}{\lambda_{P\min}}\right)^{\frac{1}{2}}\right)\right] \tag{62}$$

for all $t \ge 0$, where $\lambda_{P\min}$ is the minimum eigenvalue of P, and $\boldsymbol{y_m} = (y_m, \dot{y}_m, \ldots, y_m^{(n-1)})^T$.

2.

$$\int_0^t \|\boldsymbol{e}(\tau)\|^2 d\tau \le a + b\int_0^t |\omega(\tau)|^2 d\tau \tag{63}$$

for all $t \ge 0$, where a and b are constants, and ω is the minimum approximation error defined by Eq. (46)

3. If ω is squared integrable, that is, $\int_0^\infty |\omega(t)|^2 dt < \infty$, then $\lim_{t\to\infty}\|\boldsymbol{e}(t)\| = 0$

Design example:

The parameters of the converter are listed in **Figure 6**. Consider the following system:

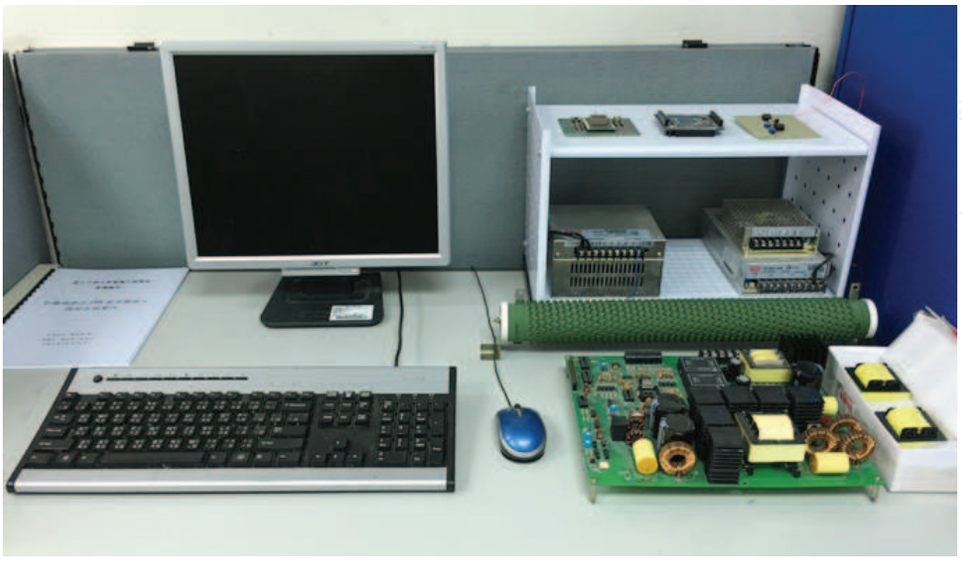

Figure 6. Photo and parameters of a PSPWM full-bridge power converter circuit. Transformer turns ratio $n = 0.5$. $V_i = 160$ volt, $V_0 = 50$ volt, $R = 6\Omega$, $C = 940\mu F$ $L = 300\mu H$, $L_{lk} = 20\mu H$ $C_A = C_B = C_C = C_D = 5nF$, $f_s = 50$ kHz.

http://dx.doi.org/10.5772/67895

$$y^{(2)} = f(\boldsymbol{x}) + g(\boldsymbol{x})u \tag{64}$$

$$f(\boldsymbol{x}) = \frac{-1}{RC^2}x_1 + \left(\frac{1}{R^2C^2} - \frac{1}{LC}\right)x_2,\ g(\boldsymbol{x}) = \frac{nv_i}{LC} \tag{65}$$

The design steps of the adaptive fuzzy controller are provided in the following:

$$\begin{aligned} u &= u_c + u_s,\ u_c = \frac{1}{\hat{g}(\boldsymbol{x}|\boldsymbol{\theta}_g)}\left[-\hat{f}(\boldsymbol{x}|\boldsymbol{\theta}_f) + y_m{}^{(2)} + \boldsymbol{k}^T\boldsymbol{e}\right] \\ u_s &= \begin{cases} \operatorname{sgn}(\boldsymbol{e}^T P\boldsymbol{b}_c)\dfrac{1}{g_L(\boldsymbol{x})}\left[|\hat{f}(\boldsymbol{x}|\boldsymbol{\theta}_f)| + |f^U(\boldsymbol{x})| + |\hat{g}(\boldsymbol{x}|\boldsymbol{\theta}_g)u_c| + |g^U(\boldsymbol{x})u_c|\right], & V_e \geq \overline{V} \\ 0, & V_e \leq \overline{V} \end{cases} \end{aligned} \tag{66}$$

Step 1:

Let

$$\Lambda_c = \begin{bmatrix} 0 & 1 \\ -100000 & -1000 \end{bmatrix}, Q = \begin{bmatrix} 200000 & 0 \\ 0 & 1 \end{bmatrix} \tag{67}$$

Use ${\Lambda_c}^T P + P\Lambda_c = -Q$ to find P

$$P = \begin{bmatrix} 1150 & 1 \\ 1 & 0.0015 \end{bmatrix}, \lambda_{P\min} = 0.00063 \tag{68}$$

Determine the range of $\boldsymbol{x}$

$$0 < x_1 < 20, 0 < x_2 < 60, 0 < \|\boldsymbol{x}\| < 63.24 \tag{69}$$

Determine the range of input and output

$$10 < u \leq 90, y_m = 50 \tag{70}$$

Obtain $\overline{V}$ by

$$\left(\frac{2\overline{V}}{\lambda_{P\min}}\right)^{\frac{1}{2}} \leq 13.24, \overline{V} = \frac{\lambda_{P\min}}{2}(13.24)^2 = 0.055 \tag{71}$$

Find $f^U(\boldsymbol{x})$, $g^U(\boldsymbol{x})$, $g_L(\boldsymbol{x})$ according to

$$\begin{aligned} |f(\boldsymbol{x})| &= \left|\frac{-1}{RC^2}x_1 + \left(\frac{1}{R^2C^2} - \frac{1}{LC}\right)x_2\right| \\ &= \left|\frac{-1}{6\times(940\times10^{-6})^2}x_1 + \left(\frac{1}{6^2(940\times10^{-6})^2} - \frac{1}{(300\times10^{-6})(940\times10^{-6})}\right)x_2\right| \\ &= 188,622.3027x_1 + 3,514,662.2403x_2 = f^U(\boldsymbol{x}) \\ |g(\boldsymbol{x})| &= \left|\frac{nv_i}{LC}\right| = \frac{0.5\times160}{(300\times10^{-6})(940\times10^{-6})} = 283,687,943.2624 = g^U(\boldsymbol{x}) = g_L(\boldsymbol{x}) \end{aligned} \tag{72}$$

Set the other parameters as

$$M_f = 1,000,000,000,\ M_g = 1,000,000,000,\ \varepsilon = 2,\ \gamma_1 = 10,000,000,000,\ \gamma_2 = 500,000,000 \quad (73)$$

Step 2:

Establish the following fuzzy rules

$$\begin{aligned} &\mu_{F_1^1}(x_1) = \exp\left(-\left(\tfrac{x_1-0}{2}\right)^2\right), \mu_{F_1^2}(x_1) = \exp\left(-\left(\tfrac{x_1-4}{2}\right)^2\right), \mu_{F_1^3}(x_1) = \exp\left(-\left(\tfrac{x_1-8}{2}\right)^2\right), \\ &\mu_{F_1^4}(x_1) = \exp\left(-\left(\tfrac{x_1-12}{2}\right)^2\right), \mu_{F_1^5}(x_1) = \exp\left(-\left(\tfrac{x_1-16}{2}\right)^2\right), \mu_{F_1^6}(x_1) = \exp\left(-\left(\tfrac{x_1-20}{2}\right)^2\right) \end{aligned} \quad (74)$$

$$\begin{aligned} &\mu_{F_2^1}(x_2) = \exp\left(-\left(\tfrac{x_1-0}{6}\right)^2\right), \mu_{F_2^2}(x_2) = \exp\left(-\left(\tfrac{x_1-12}{6}\right)^2\right), \mu_{F_2^3}(x_2) = \exp\left(-\left(\tfrac{x_1-24}{6}\right)^2\right), \\ &\mu_{F_2^4}(x_2) = \exp\left(-\left(\tfrac{x_1-36}{6}\right)^2\right), \mu_{F_2^5}(x_2) = \exp\left(-\left(\tfrac{x_1-48}{6}\right)^2\right), \mu_{F_2^6}(x_2) = \exp\left(-\left(\tfrac{x_1-60}{6}\right)^2\right) \end{aligned} \quad (75)$$

such that we have 36 rules

$$\hat{f}(\boldsymbol{x}|\boldsymbol{\theta}_f) = \boldsymbol{\theta}_f^T \xi_f(x), \hat{g}(\boldsymbol{x}|\boldsymbol{\theta}_g) = \boldsymbol{\theta}_g^T \xi_g(\boldsymbol{x}) \quad (76)$$

where

$$\xi_l(\boldsymbol{x}) = \prod_{i=1}^{2} \mu_{F_i^l}(x_i) \Big/ \sum_{l=1}^{36} \prod_{i=1}^{2} \mu_{F_i^l}(x_i), l = 1, 2 \ldots 36 \quad (77)$$

Step 3:

Use the adaptive law as described in Eq. 51 to Eq. 59

Numerical simulation is performed by augmenting the controller and parametric adaptive law with the comprehensive open-loop model. **Figure 7** is the input, output current, output

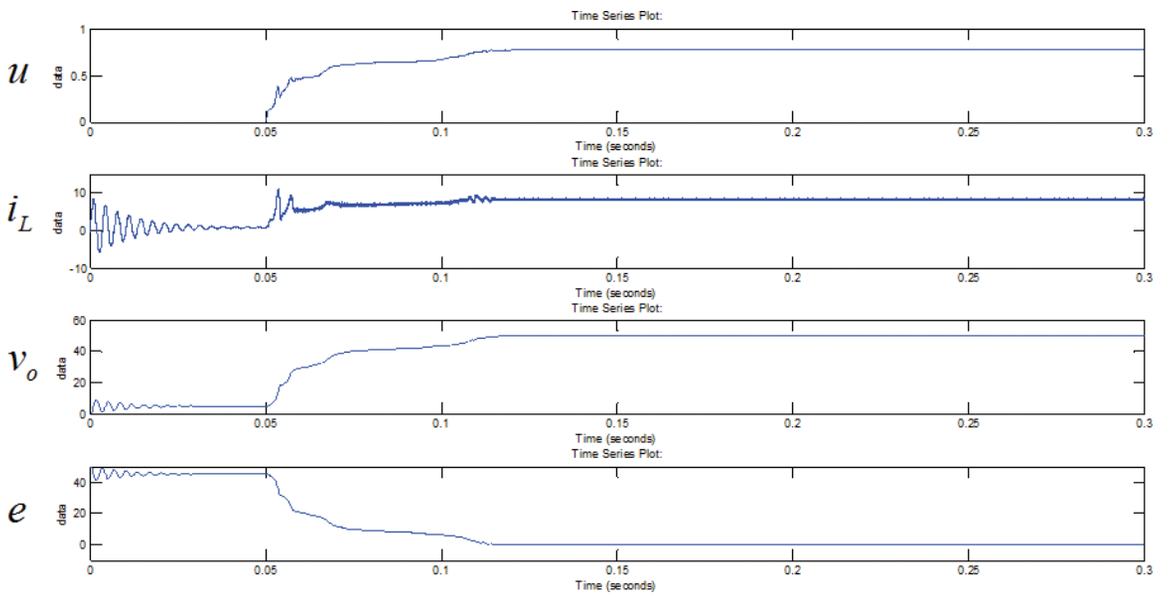

Figure 7. t = 0~0.3s.

http://dx.doi.org/10.5772/67895

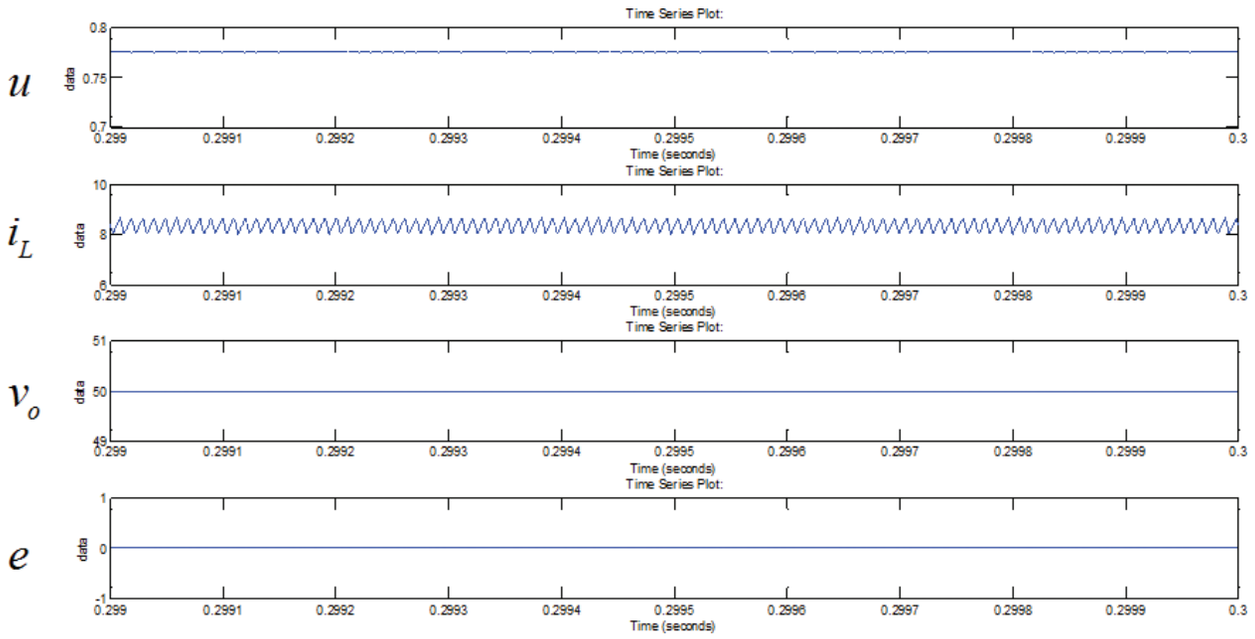

Figure 8. $t = 0.299\sim0.3$.

voltage, and tracking error within 0–0.3s. The input is not supplied until 0.05s to allow some transient response. Note that the tracking error converges around 0.12s. **Figure 8** is the zoomed input, output current, output voltage, and tracking error within 0.299–0.3s. We see that the output voltage converges to 50V and the tracking error converges to 0.

8. Conclusion

This chapter presents a control-oriented modeling and analysis approach for a class of PWM full-bridge power converters. The results can be extended to other categories of switching power converters with complex topology. The proposed modeling and analysis approach provides an assortment of essential information for subsequent control design, including selection of the values of circuit elements, stability characteristics of the open-loop system, controllable and observable signals/variables, and so on. Current research on feedback control of dc-dc power converters mostly focuses on systems with simple circuit topology (buck, boost, or buck/boost). In particular, control for soft switched PSPWM full-bridge converters is still limited to linearized design with PI or lead-lag compensators. The conventional linearized design approaches may overlook critical dynamics due to bilinear terms being neglected. For systems possessing nonlinearities and uncertainties of which accurate mathematical description is difficult to obtain, fuzzy control is definitely a sensible option. Moreover, in this study, we see that desirable properties are achieved (e.g., tracking, robustness) by integrating fuzzy control with parametric adaptation and sliding mode control. For future work, the experimental verification of the proposed control system is currently under progress. It is also a future plan to build a power factor correction (PFC) circuit to shape the input current of off-line power supplies for maximizing the actual power available from the mains. Another motivation to employ PFC is to comply with regulatory requirements.

Acknowledgements

The author gratefully acknowledges the support from the Ministry of Science and Technology, R.O.C., under grant MOST105-2221-E-005-047.

Author details

Cheng-Lun Chen

Address all correspondence to: chenc@dragon.nchu.edu.tw

National Chung Hsing University, Taiwan, Republic of China

References

[1] Mweene LH, Wright CA, Schlecht MF. A 1 kW 500 kHz front-end converter for a distributed power supply system. IEEE Transactions on Power Electronics. 1991;6(3):398–407.

[2] Redl R, Sokal NO, Balogh L. A novel soft-switching full-bridge DC/DC converter: analysis, design considerations, and experimental results at 1.5 kW, 100 kHz. IEEE Transactions on Power Electronics. 1991;6(3):408–418.

[3] Brunoro M, Vieira JLF. A high-performance ZVS full-bridge DC-DC 0-50-V/0-10-A power supply with phase-shift control. IEEE Transactions on Power Electronics. 1999;14(3):495–505.

[4] Cho J-G, Sabate JA, Hua G, Lee FC. Zero-voltage and zero-current-switching full bridge PWM converter for high-power applications. IEEE Transactions on Power Electronics. 1996;11(4):622–628.

[5] Hua G, Lee FC, Jovanovic MM. An improved full-bridge zero-voltage-switched PWM converter using a saturable inductor. IEEE Transactions on Power Electronics. 1993;8 (4):530–534.

[6] Jang Y, Jovanovic MM, editors. A new family of full-bridge ZVS converters. Applied Power Electronics Conference and Exposition, 2003 APEC'03 Eighteenth Annual IEEE; 2003: IEEE.

[7] Jang Y, Jovanovic MM, Chang Y-M. A new ZVS-PWM full-bridge converter. IEEE Transactions on Power Electronics. 2003;18(5):1122–1129.

[8] Redl R, Balogh L, Edwards DW, editors. Optimum ZVS full-bridge dc/dc converter with PWM phase-shift control: analysis, design considerations, and experimental results. Applied Power Electronics Conference and Exposition, 1994 APEC'94 Conference Proceedings 1994, Ninth Annual; 1994: IEEE Orlando, Florida (USA).

[9] Cho J-H, Seong H-W, Jung S-M, Park J-S, Moon G-W, Youn M-J, editors. Implementation of digitally controlled phase shift full bridge converter for server power supply. Energy Conversion Congress and Exposition (ECCE), 2010 IEEE; 2010: IEEE Atlanta, Georgia (USA).

[10] Lim J-G, Lim S-H, Chung S-K, editors. Digital control of phase-shifted full bridge PWM converter. 2007 ICPE'07 7th International Conference on Power Electronics; 2007: IEEE Daegu, Korea.

[11] Liu Y-F, Meyer E, Liu X. Recent developments in digital control strategies for DC/DC switching power converters. IEEE Transactions on Power Electronics. 2009;24(11):2567–2577.

[12] Tseng K-H, Chen C-L, editors. Design and hardware implementation for a full-bridge phase-shift PWM DC/DC converter system with FPGA-based PI gain-scheduling control. 2011 6th IEEE Conference on Industrial Electronics and Applications (ICIEA); 2011: IEEE Beijing, China.

[13] Schutten MJ, Torrey DA. Improved small-signal analysis for the phase-shifted PWM power converter. IEEE Transactions on Power Electronics. 2003;18(2):659–669.

[14] Vlatkovic V, Sabate JA, Ridley RB, Lee FC, Cho BH. Small-signal analysis of the phase-shifted PWM converter. IEEE Transactions on Power Electronics. 1992;7(1):128–135.

[15] Chen W, Lee FC, Jovanovic M, Sabate JA, editors. A comparative study of a class of full bridge zero-voltage-switched PWM converters. Applied Power Electronics Conference and Exposition, 1995 APEC'95 Conference Proceedings 1995, Tenth Annual; 1995: IEEE Dallas, Texas (USA).

[16] Alonge F, D'Ippolito F, Raimondi FM, Tumminaro S. Nonlinear modeling of DC/DC converters using the Hammerstein's approach. IEEE Transactions on Power Electronics. 2007;22(4):1210–1221.

[17] Ortiz CEC. On the circuit oriented average large-signal modeling of switching power converters and its applications. Virginia Polytechnic Institute and State University; 2003 Blacksburg, Virginia (this is a doctoral dissertation).

[18] Iannello C, Luo S, Batarseh I. Small-signal and transient analysis of a full-bridge, zero-current-switched PWM converter using an average model. IEEE Transactions on Power Electronics. 2003;18(3):793–801.

[19] Tsai F-S. Small-signal and transient analysis of a zero-voltage-switched, phase-controlled PWM converter using averaged switch model. IEEE Transactions on Industry Applications. 1993;29(3):493–499.

[20] Van Dijk E, Spruijt J, O'sullivan DM, Klaassens JB. PWM-switch modeling of DC-DC converters. IEEE Transactions on Power Electronics. 1995;10(6):659–665.

[21] Chen C-C, Chen C-L, Chang J-X, Yang C-F. LPV Gain-scheduling control for a phase-shifted PWM full-bridge soft switched converter. IFAC Proceedings Volumes. 2014;47(3):6135–6140.

IntechOpen